Surface modified chitosan-silica nanocomposite porous thin film based multi-parametric optical glucose sensor

Deeparati Basu[1] · Syed Minhaz Hossain[2] · Jayoti Das[1]

Abstract

In this work, a multi-parametric optical sensor based on chitosan-silica nanocomposite (CSNC) porous thin film has been developed for effective detection of glucose in pathological range. The CSNC films were surface functionalized with Glucose Oxidase enzyme via Glutaraldehyde crosslinking chains for better attachment of enzyme molecules on thin film surface. FESEM and FTIR were performed for morphological and compositional characterisation of the composite films. Five inter-linked optical parameters, i.e., transmittance (T), reflectance (R), internal scattering (IS), surface scattering (SS) and output power (OP) were measured simultaneously using image processing environment for cost efficiency of the system. Effect of surface functionalization on individual parameter response was studied. It was observed that without surface functionalization only two parameters change significantly, while surface functionalization enables all five parameters. For lower and higher glucose concentration (< 17 mM and > 17 mM), IS and SS were found to be maximum sensitive among the five parameters, respectively. Maximum sensitivity of 1.2 mM^{-1} in IS and 1 mM^{-1} in SS were observed for surface functionalized samples. The sensor showed good sensitivity, selectivity and reproducibility in the dynamic range of 3–30 mM and LOD of the sensor was found to be 0.76 mM. CSNC sensors were found suitable for single-time use and as mass production is possible with little amount of composite solution (250 sensors with just 10-ml composite solution), the sensor fabrication method is very much cost efficient. Image processing-based multi-parametric sensing is a novel field itself and detailed study of surface modified CSNC glucose sensors utilizing such sensing system is a unique work having potential to significantly contribute in the field of multi-parametric label-free optical biosensor research.

Keywords Nanocomposite · Porous thin film · Surface functionalization · Image processing · Multi-parametric glucose sensor · Interlinked parameters

1 Introduction

Label-free optical biosensors are an emerging field of research as they do not require complicated tagging procedure which often interferes with biomolecule functionality. Label-free techniques like Surface Plasmon Resonance (SPR), Interferometry, Fiber Optic sensors, Whispering Gallery structures, etc., are being investigated extensively in the last decade as they provide direct and precision measurements for different bio-analytes [1–10]. In the recent years, utilization of advanced optical techniques combined with unique sensing materials has immensely improved the performance of label-free optical biosensors making them a suitable choice for analysing a vast range of bio-analytes. Sansone et al. reported a photonic crystal deposited UV–vis optical fiber biosensor which can detect biotinylated bovine serum albumin concentration as low as 1.5fM [11]. F. Esposito et al. demonstrated long period fiber grating in double cladding fiber for potential application in vitamin D detection and obtained LOD as low as 1 ng/mL [12]. A microfluidic biosensor based on TiO$_2$ coated porous silicon was reported by S. Zhou et al. for highly sensitive S-layer protein detection using light reflection interference method [13]. A plasmonic fiber optic absorbance sensor was reported by Murugan et al. for rapid detection of SARS-COV-2 virus directly from saliva sample using gold nanoparticle-coated U-bend fiber optic probe [14]. Lee et al. demonstrated reflectance-based influenza A virus detection using biomimetic

✉ Jayoti Das
  jayoti.das@gmail.com

1 Departmemt of Physics, Jadavpur University, Kolkata, India

2 Department of Physics, IIEST Shibpur, Howrah, India

spin-on-glass nanopillar structures fabricated by nanoimprint lithography [15]. These techniques are highly sensitive; but most of them are single parametric in nature. Multi-parametric sensors are in general much more reliable than their single parametric counterparts and in optical biosensing field; such multi-parametric systems have not been reported frequently. A single optical parameter like transmittance or absorption is often not sufficient to analyse the overall phenomenon inside the sensor upon analyte introduction. Study of all the interlinked parameters like transmittance (T), reflectance (R), output power (OP), internal and surface scattering (IS and SS) together provides an overall idea of the change induced by analyte molecules. Also, for different range of analyte concentrations different parameters may show significant rise in sensitivity for nonlinear response curve and in such cases, we can choose maximum sensitive parameter for analysing that particular concentration range. So, such multi-parametric image processing-based optical sensing has the ability to produce highly sensitive and reliable results in label-free optical biosensor application.

Chitosan is a biocompatible and nontoxic linear amino polysaccharide which makes it a suitable base for biosensor devices [16, 17]. Also, large number of primary amines present in chitosan structure helps in enzyme attachment on sensor surface. Chitosan composite-based glucose sensors especially electrochemical sensors have been reported largely in the last few years [18–23], whereas only a small number of optical sensors have been investigated. Mukhtar et al. demonstrated a comparison of glucose sensitivity between Cu/Chitosan and Ag/Chitosan composite in SPR arrangement [24]. Chitosan/Silver nanocomposite was used for colorimetric detection of glucose molecule using UV–vis spectrophotometer [25]. Polypyrrole-chitosan/graphine quantum dot layers were used to detect low concentration of glucose in SPR setup [26]. Detailed study on surface modified Chitosan-Silica nanocomposite (CSNC)-based optical glucose sensor has not been reported earlier. Pure chitosan film is optically transparent but its refractive index can be modulated by controlled addition of filler components. The advantage of adding Silica nanoparticle (SiNp) fillers in chitosan matrix is that, structural stability of the film increases and swelling due to water absorption decreases which allows the film to go through repeated chemical modification steps required for surface functionalization [27]. Also, pore size of the composite film can be controlled easily by varying SiNp size; as simple hot NaOH etching dissolves surface SiNp leaving behind a negatively patterned porous composite structure. In our previous work, CSNC membrane preparation and influence of pore diameter on physiochemical properties of the freestanding membranes was reported [28]. It was found that 300 nm SiNp size was optimum for uniform pore distribution of the membranes. Also, a brief study on glucose absorption capability of the membranes

was demonstrated without any surface modification. As in the previous work, there was limited scope to discuss actual glucose sensing performance of the CSNC samples; in this new work, we have mainly focussed on detailed investigation of surface functionalized CSNC thin film glucose sensors in terms of different biosensor characteristics like sensitivity, selectivity, response time and many more. An extensive comparison between surface functionalized (SF) and non-functionalized (WSF) CSNC thin films has presented in this work which clearly demonstrates effect of surface modification on individual parameter response.

2 Experimental

2.1 CSNC thin film preparation

CSNC membrane preparation procedure has already been discussed in our previous work [28]. Here instead of free standing membranes, we have fabricated CSNC thin films on glass substrate. Initial preparation steps are same as CSNC membrane preparation. Briefly, SiNp of ~ 300 nm diameter was prepared using standard Stober's method [29] as they provide most uniform pore distribution in the CSNC samples. Next, 200-mg chitosan powder was added in 10 ml of 2% acetic acid solution and stirred vigorously until clear suspension was obtained. Then 200-mg SiNp powder was added to the solution and stirred for further 20 min. The composite solution was further ultrasonicated for 10 min to get rid of any aggregates formed in SiNp dust and again stirred for 10 min to obtain monodispersed solution. 40-µL solution was drop casted on clear cover slips (dimension: ~ 18 × 18 mm); so over 250 sensor chips can be prepared from only 10-ml composite solution making the fabrication method extremely cost efficient. The cover slips were dried at room temperature for 48 h. For etching, 5% NaOH solution was prepared and the cover slips were dipped in the solution for 40 min at 90 °C. In membrane preparation, the samples were washed in methanol solution. Here, the samples were washed vigorously in DI water and left for slow drying at room temperature for 48 h which aids strong attachment of the thin films with glass substrate.

2.2 Surface functionalization

The CSNC films were first activated by dipped them in 10 ml of 0.1% (v/v) Glutaraldehyde (GTA) solution for 2 h and washing with DI water afterwards. GTA replaces –NH$_2$ groups of chitosan with C=N groups and generates crosslinking chains which aid further attachment of enzymes on CSNC surface [30]. For enzyme immobilization, 4-mg Glucose Oxidase (GOX) powder was mixed in 10-ml phosphate buffer solution (pH 6.8) and the activated thin films

were incubated in enzyme solution for 24 h. Afterwards, the sensors were dipped in Tween20 solution and washed with phosphate buffer solution (PBS) to remove loosely attached enzymes. Effect of higher concentration of GTA and different concentrations of GOX has been discussed in Sect. 3.5 and 3.6, respectively.

2.3 Characterization

Morphological characterization of CSNC thin film sensors was performed using FESEM (FEI, INSPECT F50). For compositional characterization, i.e., investigation of functional groups present in the sensor and confirmation of enzyme attachment on CSNC surface, IR absorption spectra for 4000–400 cm^{-1} was investigated using FTIR spectroscopy.

2.4 Optical measurement

An optical breadboard arrangement in mini darkroom environment was utilized for image processing-based multi-parametric measurements [28]. Red LASER (630 nm, 5mW, Holmarc) was used as optical source which falls obliquely on sensor surface (Fig. 1). Spot size of the laser on sensor surface was set around 2–3 mm. Transmitted and reflected components of the laser beam from sensor film falls on screen arrangement and images of these two spots were captured by CMOS camera. MATLAB image processing environment was used to obtain Intensity Distribution Matrix (IDM) of the spot images and further processing produced 3D Gaussian model corresponding to the IDMs. The peak intensity

of this Gaussian for transmitted IDM gives transmittance value (T) and Full Width Half Maxima (FWHM) gives a measurement of Internal Scattering (IS) within the sensor film. Similarly peak intensity of the Gaussian obtained from reflected IDM gives reflectance value (R) and FWHM gives a measurement of Surface Scattering (SS). Now, the total 3D volume under the two Gaussian plots (for transmitted and reflected spot) gives a measurement of the optical power coming out of the sensor which is our fifth parameter named as Output Power (OP) that gives an understanding of optical absorption within the sensor film.

For sensor measurements, initially baseline data were collected before glucose introduction. Then, 0.25 ml of glucose solution was sprayed and %Response change on the baseline data was observed. Relative response of the five parameters is defined as,

$$\% \textbf{Response} = \left| \frac{(V_f - V_0)}{V_0} \right| \times 100\% \qquad (1)$$

where, $V_0 =$ Baseline value of any of the five parameters. $V_f =$ Parameter value after glucose introduction.

3 Results and discussion

3.1 FESEM

FESEM micrographs in Fig. 2a show even pore distribution on CSNC surface after NaOH etching. Surface pore size distribution analysis (Fig. 2e) obtained from FESEM
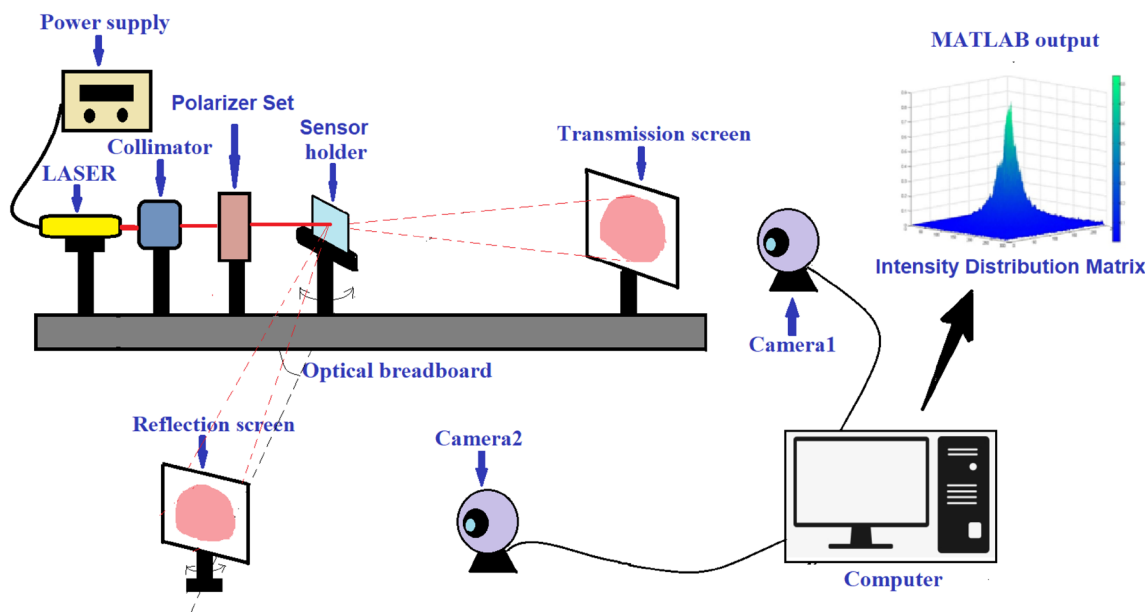

Fig.1 Schematic diagram of multi-parametric optical measurement setup
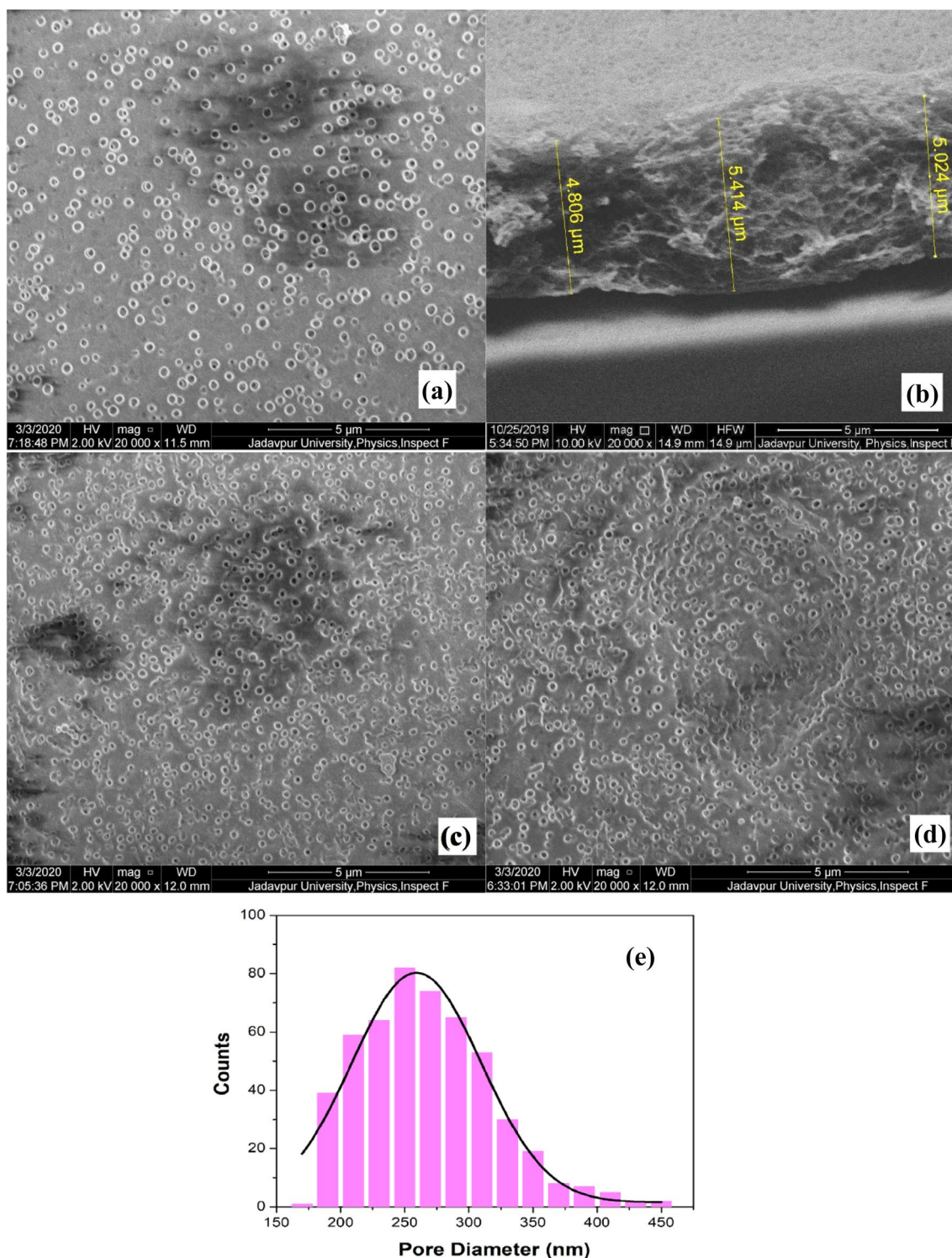
Fig.2 FESEM micrograph of **a** CSNC film top view, **b** CSNC film cross section, **c** GOX modified CSNC film and **d** GOX modified film after glucose solution introduction. **e** Surface pore size distribution of CSNC films (obtained from FESEM micrograph **a**)

micrograph of the CSNC film (Fig. 2a) shows that pore diameter range of the film is ∼ 200–320 nm with a peak pore diameter value at ∼ 260 nm. Also, surface pore density was found to be ∼ 2.7/ μm^2. From the cross sectional view (Fig. 2b), approximate thickness of the drop casted films were found to be 4.7–5.5 µm and a sponge like internal

structure was also observed. At the time of etching, first SiNps on the top surface are attacked and external surface pores are generated. Then with time, hot NaOH flows through the pores and dissolves the internal SiNps producing numerous interlinked channels, thus finally generating a sponge like net structure. Shrinkage of pore size was observed after GOX and glucose molecule attachment shown in Fig. 2c, d, respectively.

3.2 FTIR

In Fig. 3a, broad peak around 3550–3200 cm^{-1} is produced due to intermolecular O–H group stretching in chitosan polymer chain. Also peak at ~3454 cm^{-1} indicates presence of N–H bond stretching of primary amine. Absorption band in
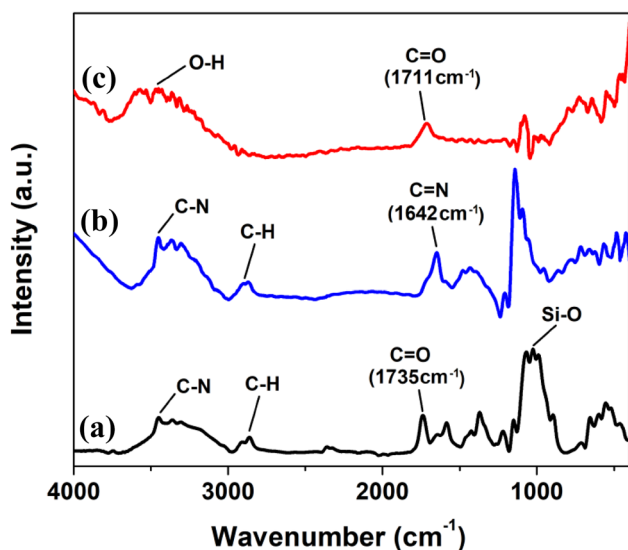

Fig.3 FTIR spectra of **a** pure CSNC film, **b** GOX modified CSNC film and **c** GOX modified film after glucose introduction

800–1260 cm^{-1} range is described as different SiO$_2$ peaks of SiNp and residual organic groups [31]. Absorption peak at ~1735 cm^{-1} represents C=O stretching of carboxylic acid which in this case is acetic acid present in composite solution mixture discussed in Sect. 2.2. For GOX functionalised surface in Fig. 3(b), absence of 1735 cm^{-1} carbonyl group peak and existence of strong imine (C=N) group peak at ~1642 cm^{-1} is observed. This indicates successful attachment of GOX molecules into CSNC film because in surface functionalization process all the carbonyl groups are replaced by imine groups [30]. After introduction of glucose solution, again the C=O stretching peak of carboxylic acid appears at ~1711 cm^{-1} in Fig. 3c which indicates further generation of gluconic acid in GOX sites [32]. 1720–1706 cm^{-1} is reported to be the band for carboxylic acid dimers and in anhydrous form, gluconic acid crystals forms dimers which indicates the presence of gluconic acid crystals in the sensor film upon evaporation of liquid analyte solution.

3.3 MATLAB Output

Transmitted and reflected spot IDMs were analysed to find the change in five parameters due to glucose absorption on GOX functionalised CSNC samples. Figure 4 shows 2D IDM plot of transmitted spot before and after 30 mM glucose absorption. From the corresponding Gaussian fit plots in Fig. 5, it is clearly visible that T increases and IS decreases due to glucose absorption. From cross-sectional view of FESEM micrograph we see presence of sponge like internal structure in CSNC films. With glucose introduction interlinked channels become filled with glucose molecules thus reducing inter-channel light propagation or scattering. This may be the effect of reduced IS value and more focussed beam than air filled channels, which in turn increases T value.
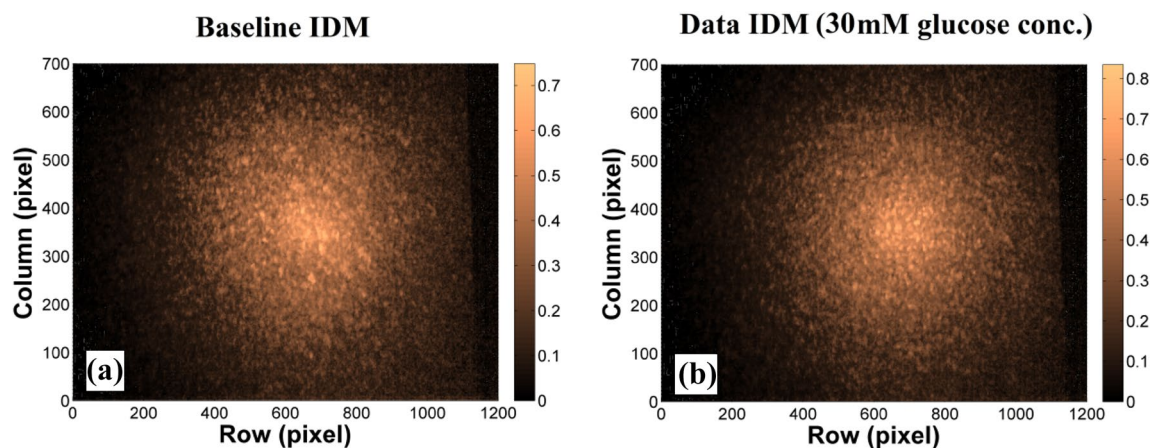

Fig.4. 2D IDM plot of **a** baseline snapshot and **b** snapshot after 30 mM glucose introduction for transmitted spot
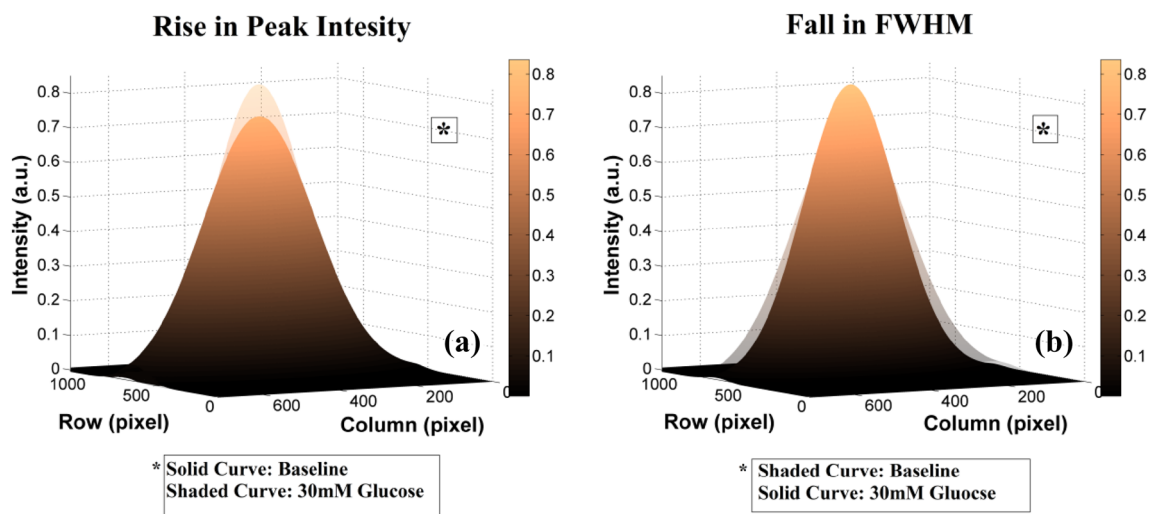
Rise in Peak Intesity

Fall in FWHM

* Solid Curve: Baseline
Shaded Curve: 30mM Glucose

* Shaded Curve: Baseline
Solid Curve: 30mM Gluocse

Fig.5. 3D Gaussian model for understanding **a** peak intensity rise and **b** FWHM fall of transmitted spot after 30 mM glucose introduction

On the other hand, from reflected spot IDM and Gaussian fit (Fig. 6 and Fig. 7, respectively), it can be observed that R decreases and SS increases due to glucose absorption. This is due to the fact that surface scattering increases with clustered attachment of glucose molecules around GOX sites on sensor surface. Increase in clustered attachment of glucose on GOX molecules, increases surface roughness significantly [33] thus increasing SS value which in turn reduces specular reflectance or R value. Also we have observed that OP increases with glucose introduction, thus we can conclude that optical absorption falls due to the presence of glucose molecules in CSNC samples.

Change in different parameters due to glucose introduction is listed in table 1 Rise and fall of actual data from baseline value is denoted with '↑' and '↓' signs, respectively. Also, for samples with and without GOX functionalization, we found the parameter change pattern was same.

3.4 Sensitivity

From the response curve for surface functionalized (SF) and non-functionalized (WSF) samples in Fig. 8, it is quite clear that all the five parameters changes significantly for SF samples, while for WSF samples only two parameters (T and IS) are significant. When glucose solution is sprayed on WSF samples, glucose molecules are evenly deposited on the top surface. As R and SS are mainly surface properties, they are not affected much. Mainly the pores of WSF samples fills with glucose molecules thus changing internal properties like T and IS significantly. In SF samples, clustered attachment of glucose molecules on GOX sites changes R and SS along with other parameters. Pores in SF samples are partially filled with GOX molecules at the time of enzyme incubation. So there is a limit up to which the pores can accommodate glucose molecules and after that limit T and
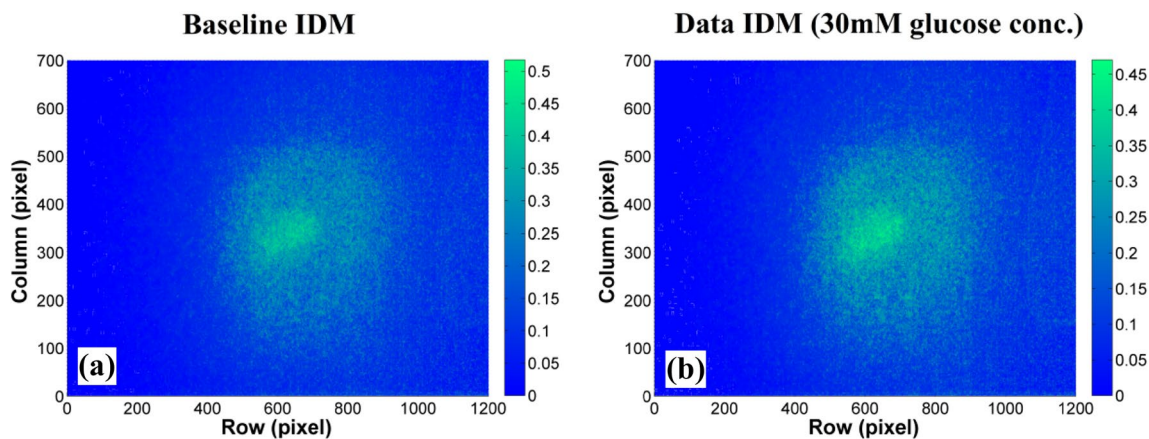
Baseline IDM

Data IDM (30mM glucose conc.)

Fig.6. 2D IDM plot of **a** baseline snapshot and **b** snapshot after 30 mM glucose introduction for reflected spot

Fall in Peak Intensity

Rise in FWHM

* | **Shaded Curve: Baseline**
  | **Solid Curve: 30mM Glucose**

* | **Solid Curve: Baseline**
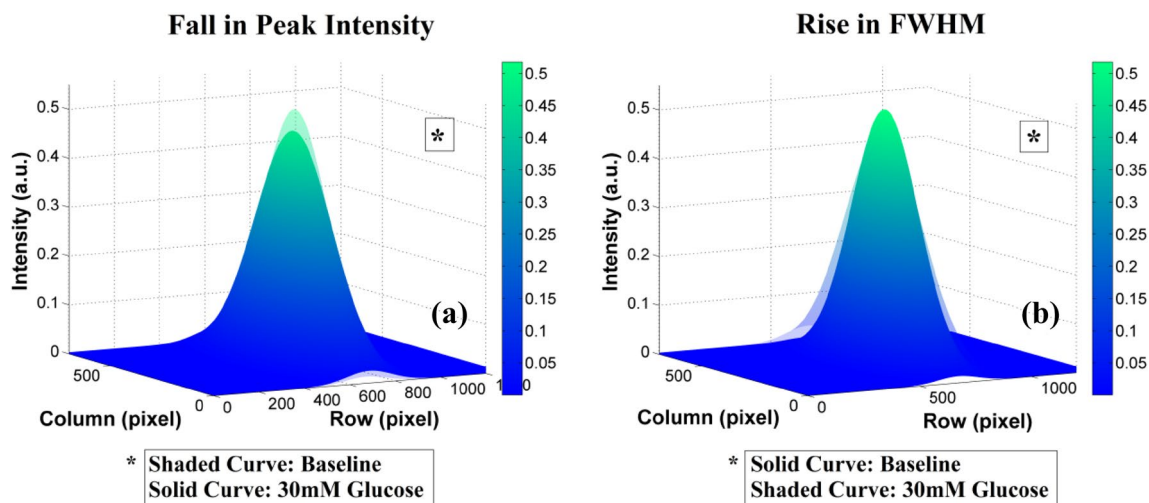 | **Shaded Curve: 30mM Glucose**

Fig.7. 3D Gaussian model for understanding **a** peak intensity fall and **b** FWHM rise of reflected spot after 30 mM glucose introduction

Table 1 Actual change in parameter readings with glucose introduction

Transmittance (T)	Internal scattering (IS)	Reflectance (R)	Surface scattering (SS)	Output power (OP)	Absorption
↑	↓	↓	↑	↑	↓

IS will be unaffected by further increase in glucose concentration. This is observed in Fig. 8b, i.e., after 17 mM glucose concentration IS almost saturates and further deposition of glucose molecules only affects T a little which may be dominated by the effect of other three parameters. So, we can conclude that SF samples are much more reliable than WSF samples for multi-parametric measurement and surface

functionalization actually introduces more parameters thus more sensitivity in the system.

As we measure deviation from baseline to calculate %Response, blank data get eliminated in each measurement. But diode laser have intensity fluctuation and CMOS sensors also have some inbuilt noise which affects the final response due to deviation in blank data, thus increasing LOD of the system. Minimum LOD was found to be 0.76 mM ($n = 10$) for SF samples considering $S/N \geq 3$. So, components like diode lasers and CMOS sensors make the multi-parametric system cost efficient compromising LOD a little. Using stable laser sources like He–Ne instead of diode lasers can reduce LOD level further. We have tested the sensor for 1–30 mM glucose concentration and determined the dynamic range to be 3–30 mM for reliable operation. Also
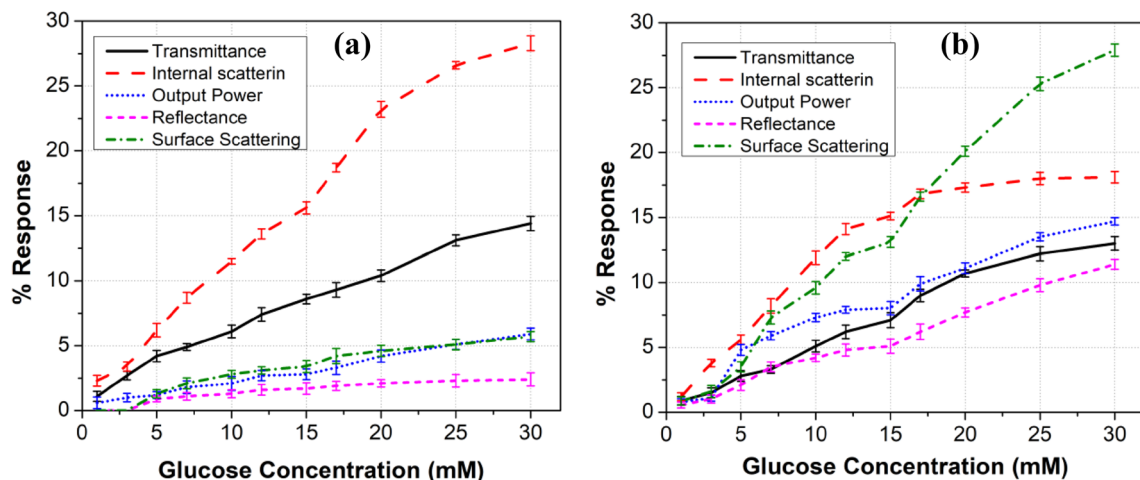

Fig.8 Response curve of CSNC samples **a** without surface functionalization (WSF) and **b** with surface functionalization (SF). Tested for 1–30 mM glucose concentration ($n = 3$)

sensitivity (%Response/Glucose concentration) was calculated for SF samples and plotted in Fig. 9. It is observed that in the range of 0-17 mM, IS is maximum sensitive among all the five parameters and maximum sensitivity value of IS was found to be 1.2 mM^{-1}. For 17–30 mM glucose concentration range, IS sensitivity was observed to fall significantly. In this range, SS was found to be the maximum sensitive parameter with sensitivity value of 1 mM^{-1}. So it can be concluded that scattering parameters are more sensitive than direct intensity-related parameters like transmittance, reflectance, absorbance, etc., which are generally measured in standard optical biosensors.

3.5 Effect of GTA concentration

GTA concentration was varied from 0.1 to 0.6% (v/v) and change in T and R for 15 mM glucose solution was observed. From Fig. 10, it is evident that above 0.2% (v/v) GTA concentration, T and R value decreases which indicates reduction of GOX enzyme activity similar to the study reported by Susanto et al. [34]. In Fig. 11, colour change of the CSNC films is clearly visible with increase in GTA concentration. Above 0.2% (v/v) GTA concentration the CSNC films become dark yellow and brittle. Also, crack lines are formed easily and often the films get detached from glass substrates. So, we have used 0.1% (v/v) GTA concentration which produced sufficiently high response.

3.6 Effect of GOX concentration

GOX concentration was also varied from 0.1 mg/ml to 0.8 mg/ml for 15 mM glucose solution. It can be observed from Fig. 12 that above 0.4 mg/ml T falls and R almost
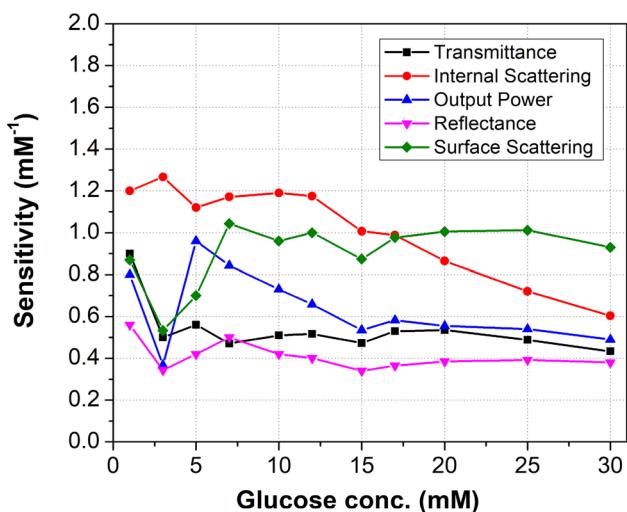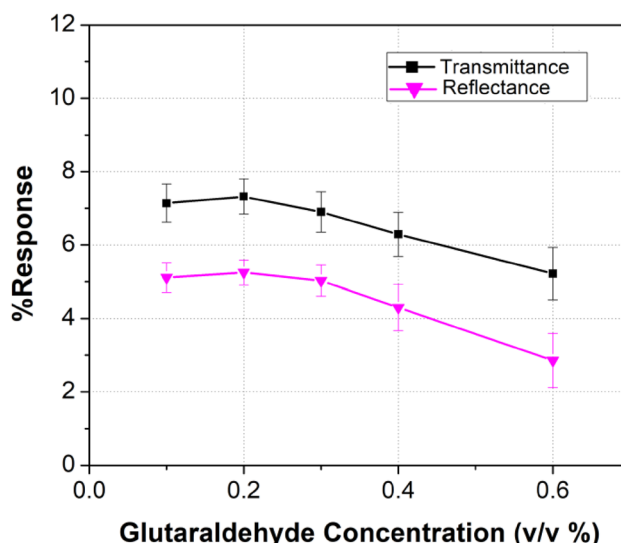

Fig.10 Effect of GTA concentration on sensor response (15 mM glucose conc., $n = 3$)

saturates. This may be because with higher GOX concentration the pores are almost filled with GOX molecules leaving less active site for glucose interaction inside the pores and T becomes less sensitive. On the other hand, when surface of the CSNC film is totally covered with GOX molecules number of active sites will saturate on the surface and so as R value. Thus, 0.4 mg/ml GOX concentration was considered for optimum performance of the sensor.

3.7 Selectivity

For selectivity study 15 mM glucose, fructose, galactose, maltose and sucrose solutions were prepared. Also, phosphate buffer (PBS) was used as control. WSF and SF samples were tested for different analyte solutions. It was observed from Fig. 13a that WSF samples show quite high response for all the solutions except PBS control which is expected because WSF surface has no GOX enzyme present to selectively attract glucose molecules. Thus all the analytes either gets absorbed inside the pores or attaches to the surface while solution evaporation process. There is an

Fig.9 Sensitivity plot for surface functionalized (SF) samples (calculated from the mean response values obtained from response curve)

Fig.11 Visual effect of increased GTA concentration on CSNC thin films (standard cover slips have a dimension of ∼ 18 × 18 mm and the thin films were found to have diameter of ∼ 8 mm)
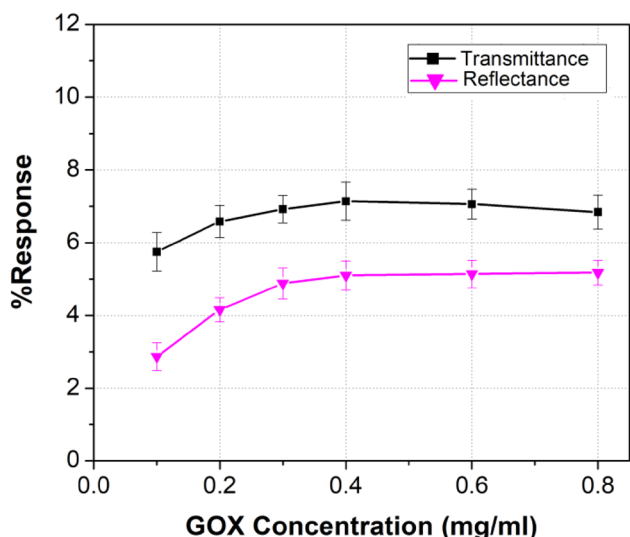
Fig.12 Effect of GOX concentration on sensor response (15 mM glucose conc., $n=3$)

interesting fact to note that glucose, fructose and galactose produces almost same pattern of output response, i.e., high values for T and IS and low value for R and SS. The reason behind such pattern is discussed in Sect. 3.4. for WSF samples. Maltose and sucrose produces significant increase in R and SS value which may be described as the effect of their molecular weight. Maltose and sucrose are disaccharides having almost double molecular weight than glucose, fructose and galactose. So their attachment to surface affects the surface roughness more than the monosaccharides and their tendency to penetrate deep inside the pores is also less likely. Thus such pattern difference in WSF sensor output is observed for different analytes. On the other hand for SF samples GOX selectively binds to glucose molecules and other analytes mostly flows down the sensor surface after

solution spray without significant absorption or attachment to the sensor. So SF samples show high selectivity towards glucose molecules (Fig. 13b).

3.8 Response time (τ)

Actual peak intensity value of the transmitted and reflected spot is monitored for 3 min time span to observe response time of the sensor. Initially baseline value of T and R was at ~ 0.79 a.u. and ~ 0.54 a.u., respectively. Baseline data fluctuation mentioned in Sect. 3.4. is also visible in time response plot (Fig. 14). After 15 mM glucose solution spray at 20 s, both T and R value reaches to maximum intensity saturation level of 1 a.u. due to lensing effect produced by water [28]. As the sensors were mounted vertically, excess solution quickly flows down and CSNC thin film starts drying. After 60 s, we see abrupt fall in T and R value and at around 80-s sensor output stabilises to new values indicating complete drying of the thin film. It can be observed that T has reached a higher value and R has reached a lower value compared to their baseline value which was demonstrated in table 1. From time response curve, it was concluded that τ is approximately 50 s for the multi-parametric sensor.

3.9 Repeatability

Repeatability study was performed on five CSNC sensors and after every cycle the sensors were washed in Tween20 solution followed by PBS buffer. It was found that in second cycle T and R response drops to 68% and 83% of the first cycle response, respectively (Fig. 15). Significant drop in T response indicates that gluconic acid crystals are not completely removed from complex sponge structure of the porous film even after vigorous washing. Also chitosan dissolves slowly in acidic solution which can produce crater like structure shown in the FESEM image in Fig. 15b. So
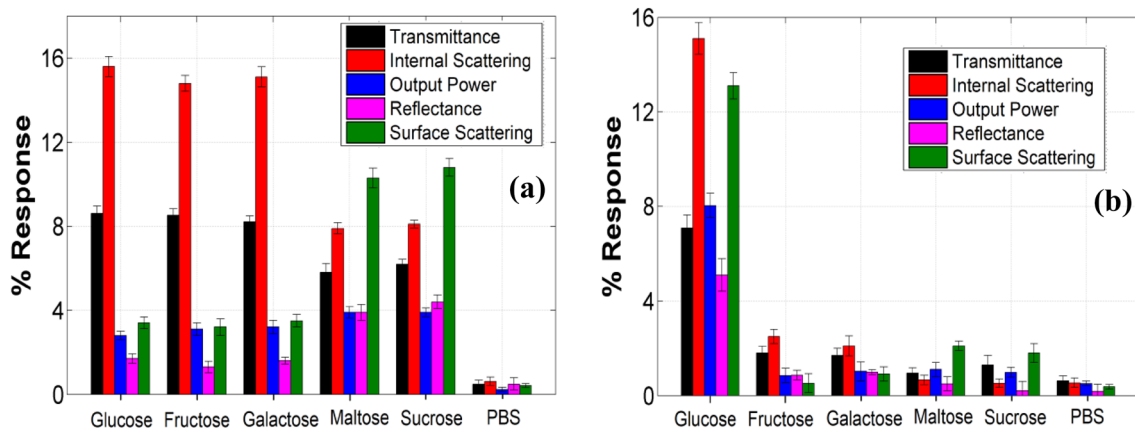

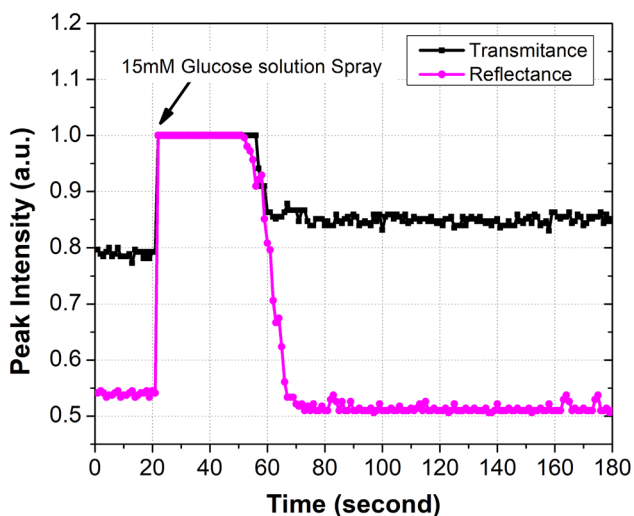**Fig.13** Selectivity of **a** WSF and **b** SF samples ($n=3$)

Fig. 14 Time response curve of CSNC sensor

with gluconic acid production and washing, the films slowly degrade thus reducing both T and R response. In third cycle, almost no significant change in output response is observed from which it is clear that the CSNC sensors are suitable only for one time use.

3.10 Stability

CSNC sensors were stored in refrigerator at 4 °C and response for 15 mM glucose solution was studied for every alternate day. 15 mM glucose solution was freshly prepared every day and new CSNC samples were taken for every measurement as the sensors are for one time use only. It was observed that after 9th day T response falls rapidly while R response shows slow degradation for SF samples shown
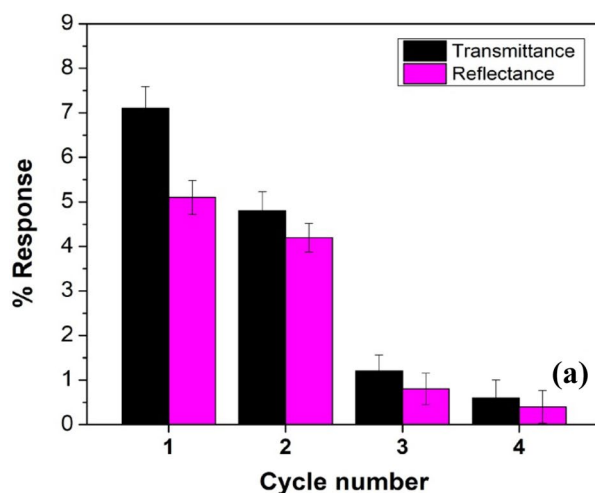
in Fig. 16b. So it can be concluded that the trapped GOX molecules inside sponge like network are affected greatly by environmental conditions compared to the surface GOX molecules. In the absence of active GOX enzyme, the sensor should act like WSF samples, but even for such samples we should get significant T response. Here we observe that T response falls to almost blank data level which can only be described by structural degradation of CSNC membranes with time. For WSF samples such degradation was not observed and up to 30 days, we get almost same response value (Fig. 16a). So, it can only lead to the conclusion that the surface functionalization steps make the sensor structure prone to degradation within 10–15 days.

4 Conclusion

Surface modified CSNC thin film sensors have been fabricated and tested in multi-parametric optical detection environment for glucose sensing. In pathological range of 3–30 mM, the sensor showed good sensitivity and selectivity. For different glucose concentration range scattering parameters IS and SS proved to be maximum sensitive among all the five parameters. Surface functionalization enables all the five parameters for much reliable sensing performance while non-functionalized sensors only provide two parameters. The sensors were suitable for single time use and response time (~ 50 s) was found quite low. So CSNC porous thin film glucose sensors have the potential to provide sensitive, reliable and cost effective measurements in pathological range for optical multi-parametric analysis.
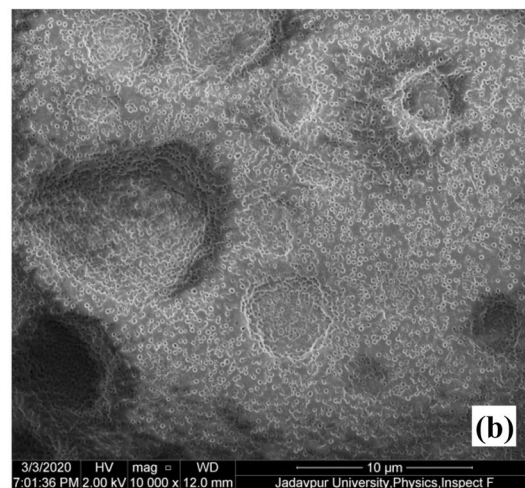

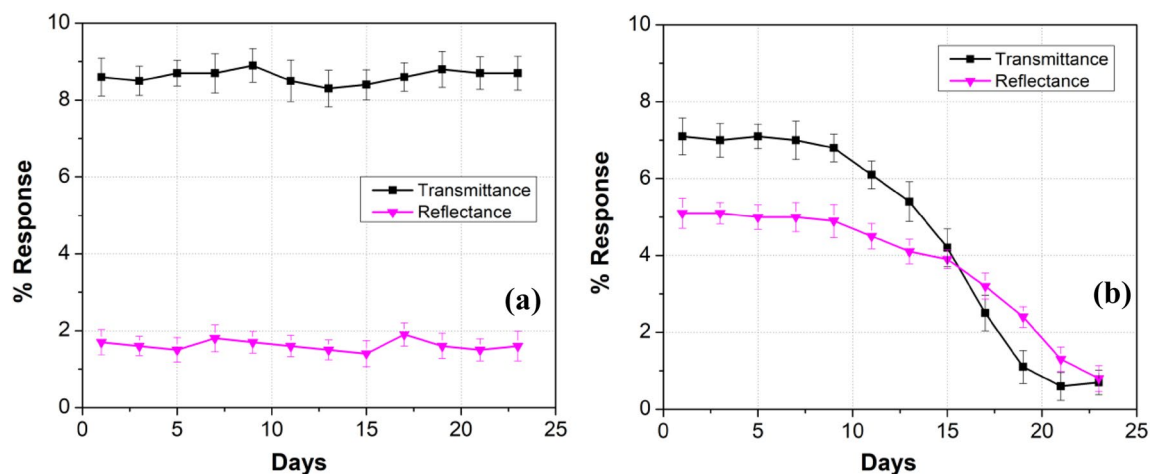**Fig.15** **a** Repeatability test for 15 mM glucose solution ($n = 5$), **b** FESEM micrograph after 3rd cycle

Fig.16 Storage stability of **a** WSF CSNC sensors and **b** SF CSNC sensor ($n = 3$)

Declarations

Conflict of interest The authors declare that there are no known conflicts of interest associated with the work presented here and there has been no significant financial support for this work that could have influenced its outcome.

References

1. X. Jiang, Y. Chen, F. Yu, L. Tang, M. Li, J.J. He, High-sensitivity optical biosensor based on cascaded Mach-Zehnder interferometer and ring resonator using Vernier effect. Opt. Lett. **39**, 6363–6366 (2014). https://doi.org/10.1364/OL.39.006363

2. S.P. Usha, B.D. Gupta, Urinary p-cresol diagnosis using nanocomposite of ZnO/MoS2 and molecular imprinted polymer on optical fiber based lossy mode resonance sensor. Biosens. Bioelectron. **101**, 135–145 (2018). https://doi.org/10.1016/j.bios.2017.10.029

3. A. Loiseau, L. Zhang, D. Hu, M. Salmain, Y. Mazouzi, R. Flack, B. Liedberg, S. Boujday, Core–shell gold/silver nanoparticles for localized surface Plasmon resonance-based naked-eye toxin biosensing. ACS Appl. Mater. Interfaces. **11**(50), 46462–46471 (2019). https://doi.org/10.1021/acsami.9b14980

4. A. Lokman, S.W. Harun, Z. Harith, H.A. Rafaie, R.M. Nor, H. Arof, Inline Mach-Zehnder interferometer with ZnO nanowires coating for the measurement of uric acid concentrations. Sens Actuators A **234**, 206–211 (2015). https://doi.org/10.1016/j.sna.2015.09.013

5. M.D. Baaske, M.R. Foreman, F. Vollmer, Single-molecule nucleic acid interactions monitored on a label-free microcavity biosensor platform. Nat. Nanotechnol. **9**(11), 933–939 (2014). https://doi.org/10.1038/nnano.2014.180

6. M. Bahadoran, A.F.A. Noorden, K. Chaudhary, F.S. Mohajer, M.S. Aziz, S. Hashim, J. Ali, P. Yupapin, Modeling and analysis of a microresonating biosensor for detection of *Salmonella*

7. B.T. Wang, Q. Wang, An interferometric optical fiber biosensor with high sensitivity for IgG/anti-IgG immunosensing. Optics Commun **426**, 388–394 (2018). https://doi.org/10.1016/j.optcom.2018.05.058

8. S.K. Srivastava, V. Arora, S. Sapra, B.D. Gupta, Localized surface plasmon resonance-based fiber optic U-shaped biosensor for the detection of blood glucose. Plasmonics **7**(2), 261–268 (2012). https://doi.org/10.1007/s11468-011-9302-8

9. G. Wandermur, D. Rodrigues, R. Allil, V. Queiroz, R. Peixoto, M. Werneck, M. Miguel, Plastic optical fiber-based biosensor platform for rapid cell detection. Biosens Bioelectron. **54**, 661–666 (2014). https://doi.org/10.1016/j.bios.2013.11.030

10. J. Maldonado, M.-C. Estévez, A. Fernández-Gavela, J.J. González-López, A.B. González-Guerrero, L.M. Lechuga, Label-free detection of nosocomial bacteria using a nanophotonic interferometric biosensor. Analyst **145**(2), 497–506 (2020). https://doi.org/10.1039/C9AN01485C

11. L. Sansone, E. Macchia, C. Taddei, L. Torsi, M. Giordano, Label-free optical biosensing at femtomolar detection limit. Sens Actuators B Chem. **255**, 1097–1104 (2018). https://doi.org/10.1016/j.snb.2017.08.059

12. F. Esposito, L. Sansone, A. Srivastava, A.M. Cusano, S. Campopiano, M. Giordano, A. Iadicicco, Label-free detection of vitamin D by optical biosensing based on long period fiber grating. Sens Actuators B Chem. **347**, 130637 (2021). https://doi.org/10.1016/j.snb.2021.130637

13. S. Zhuo, M. Xun, M. Li, X. Kong, R. Shao, T. Zheng, D. Pan, J. Li, Q. Li, Rapid and label-free optical assay of S-layer protein with high sensitivity using TiO2-coated porous silicon-based microfluidic biosensor. Sens Actuators B Chem. **321**, 128524 (2020). https://doi.org/10.1016/j.snb.2020.128524

14. D. Murugan, H. Bhatia, V.V.R. Sai, J. Satija, P-FAB: a fiber-optic biosensor device for rapid detection of COVID-19. Trans Indian Natl Acad Eng **5**(2), 211–215 (2020). https://doi.org/10.1007/s41403-020-00122-w

15. W.S. Lee, J. Ahn, S. Jung, J. Lee, T. Kang, J. Jeong, Biomimetic nanopillar-based biosensor for label-free detection of influenza A virus. BioChip J. **15**(3), 260–267 (2021). https://doi.org/10.1007/s13206-021-00027-y

16. C. Peniche, W. Argüelles-Monal, H. Peniche, N. Acosta, Chitosan: an attractive biocompatible polymer for microencapsulation.

Macromol. Biosci. **3**(10), 511–520 (2003). https://doi.org/10.1002/mabi.200300019

17. G. Kravanja, M. Primožič, Ž Knez, M. Leitgeb, Chitosan-based (Nano) materials for novel biomedical applications. Molecules **24**(10), 1960 (2019). https://doi.org/10.3390/molecules24101960

18. D. Feng, F. Wang, Z. Chen, Electrochemical glucose sensor based on one-step construction of gold nanoparticle–chitosan composite film. Sens Actuators B Chem. **138**(2), 539–544 (2009). https://doi.org/10.1016/j.snb.2009.02.048

19. J. Zhu, Z. Zhu, Z. Lai, R. Wang, X. Guo, X. Wu, G. Zhang, Z. Zhang, Y. Wang, Z. Chen, Planar amperometric glucose sensor based on glucose oxidase immobilized by chitosan film on Prussian blue layer. Sensors **2**(4), 127–136 (2002). https://doi.org/10.3390/s20400127

20. N. Khalaf, T. Ahamad, M. Naushad, N. Al-Hokbany, S.I. Al-Saeedi, S. Almotairi, S.M. Alshehri, Chitosan polymer complex derived nanocomposite (AgNPs/NSC) for electrochemical non-enzymatic glucose sensor. Int J Biol Macromol. **146**, 763–772 (2020). https://doi.org/10.1016/j.ijbiomac.2019.11.193

21. M. Yang, Y. Yang, B. Liu, G. Shen, R. Yu, Amperometric glucose biosensor based on chitosan with improved selectivity and stability. Sens Actuators B Chem. **101**(3), 269–276 (2004). https://doi.org/10.1016/j.snb.2004.01.003

22. F. Wang, X. Ding, X. Niu, X. Liu, W. Wang, J. Zhang, Green preparation of core-shell Cu@ Pd nanoparticles with chitosan for glucose detection. Carbohyd. Polym. **247**, 116647 (2020). https://doi.org/10.1016/j.carbpol.2020.116647

23. M. Figiela, M. Wysokowski, M. Galinski, T. Jesionowski, I. Stepniak, Synthesis and characterization of novel copper oxide-chitosan nanocomposites for non-enzymatic glucose sensing. Sens Actuators B Chem. **272**, 296–307 (2018). https://doi.org/10.1016/j.snb.2018.05.173

24. W.M. Mukhtar, N.A.M. Taib, A.R.A. Rashid, Sensitivity analyses of Cu/Chitosan and Ag/Chitosan based SPR biosensor for glucose detection. J Phys Conf Ser **1892**, 012021 (2021)

25. M. Maruthupandy, G. Rajivgandhi, T. Muneeswaran, T. Vennila, F. Quero, J.M. Song, Chitosan/silver nanocomposites for colorimetric detection of glucose molecules. Int. J. Biol. Macromol. **121**, 822–828 (2019). https://doi.org/10.1016/j.ijbiomac.2018.10.063

26. A.R. Sadrolhosseini, S.A. Rashid, N. Jamaludin, A.S.M. Noor, A.M. Isloor, Surface plasmon resonance sensor using polypyrrole-chitosan/graphene quantum dots layer for detection of sugar. Mater Res Expr **6**(7), 075028 (2019)

27. Y. Liu, Z. Cai, L. Sheng, M. Ma, Q. Xu, Influence of nanosilica on inner structure and performance of chitosan based films. Carbohyd. Polym. **212**, 421–429 (2019). https://doi.org/10.1016/j.carbpol.2019.02.079

28. D. Basu, K. Sen, S.M. Hossain, J. Das, Influence of pore diameter on physical and sensing properties of free-standing Chitosan-Silica Nanocomposite membrane. J. Porous Mater. **28**(5), 1595–1607 (2021). https://doi.org/10.1007/s10934-021-01079-z

29. W. Stober, A. Fink, E. Bohn, Controlled growth of monodisperse silica spheres in the micron size range. J. Colloid Interface Sci. **26**, 62–69 (1968)

30. N.R. Kild'eeva, P.A. Perminov, L.V. Vladimirov, V.V. Novikov, S.N. Mikhailov, Mechanism of the reaction of glutaraldehyde with chitosan. Russ J Bioorg Chem. **35**(3), 360–369 (2009). https://doi.org/10.1134/S106816200903011X

31. A. Beganskienė, V. Sirutkaitis, M. Kurtinaitienė, R. Juškėnas, A. Kareiva, FTIR, TEM and NMR investigations of Stöber silica nanoparticles. Mater Sci (Medžiagotyra) **10**, 287–290 (2004). https://doi.org/10.5755/j01.ms.10.4.26643

32. C.M. Wong, K.H. Wong, X.D. Chen, Glucose oxidase: natural occurrence, function, properties and industrial applications. Appl. Microbiol. Biotechnol. **78**(6), 927–938 (2008). https://doi.org/10.1007/s00253-008-1407-4

33. D. Basu, T. Sarkar, K. Sen, S.M. Hossain, J. Das, Multi-Parametric optical glucose sensor based on surface functionalized nanoporous silicon. IEEE Sens J. **18**(24), 9940–9947 (2018). https://doi.org/10.1109/JSEN.2018.2872846

34. H. Susanto, A.M. Samsudin, N. Rokhati, I.N. Widiasa, Immobilization of glucose oxidase on chitosan-based porous composite membranes and their potential use in biosensors. Enzyme Microb Technol. **52**(6–7), 386–392 (2013). https://doi.org/10.1016/j.enzmictec.2013.02.005